

# Investigation of the Thermal Aging Behavior of Pyrotechnic Tracer Composition by Spectroscopic Techniques Coupled with Principal Component Analysis

Slimane Bekhouche,<sup>[a]</sup> Djalal Trache,<sup>\*[a]</sup> Salim Chelouche,<sup>[a]</sup> Amir Abdelaziz,<sup>[a]</sup> Ahmed Fouzi Tarchoun,<sup>[a, b]</sup> Widad Benchaa,<sup>[a]</sup> Sabine Benameur,<sup>[a]</sup> and Abderrahmane Mezroua<sup>[a]</sup>

**Abstract:** This work aims to investigate the aging behavior related to heat of a pyrotechnic tracer composition (PTC) sample composed of strontium nitrate as an oxidizer and dual-fuel of Mg and Mg–Al alloy. Fresh and thermally aged samples were examined using nondestructive spectroscopic techniques, namely Raman spectroscopy, scanning electron microscopy (SEM), Fourier transform infrared spectroscopy (FTIR), and X-ray diffraction (XRD). The obtained results showed that aging for 20, 40, and 60 days at 65 °C does not provoke noticeable chemical or structural changes, whereas, after 60 days, the changes are visible, and become more obvious after aging for 120 days. These

changes are caused by the partial decomposition of strontium nitrate and the oxidation of magnesium, which are followed by the generation of degradation products such as  $\text{Sr}(\text{NO}_2)_2$ ,  $\text{MgO}$ , and  $\text{Mg}(\text{OH})_2$ . On the other hand, the applicability of FTIR and XRD associated with a chemometric tool, the principal component analysis, as a simple and useful technique has been also assessed to discriminate the spectra of the aged samples. It has been revealed that these combined approaches can be effectively used to recognize the main compositional and structural changes within the pyrotechnic tracer composition affected by the thermal degradation process.

**Keywords:** Pyrotechnic tracer composition · FTIR · Raman · XRD · PCA · Accelerated aging

## 1 Introduction

Nowadays, pyrotechnic compositions which are usually constituted of inorganic or organic chemical fuels and oxidizers to generate mechanical, audible, thermal, or visual terminal effects such as motion, sound, color, light, and smoke, find a wide range of use in both civil and military applications owing to their low cost, compactness, reliability, and simplicity [1,2]. However, similar to the most common energetic materials such as propellants and explosives [3–5], pyrotechnic compositions may undergo degradation, and hence their storage life is negatively affected [6]. Their performance, reliability, and safety can be compromised by various factors such as temperature, humidity, vibration, shock, and other environmental hazards, leading to ineffective output, ignition failures, or accidental initiations during production, handling, transport, storage, and use [7,8]. Hence, it is tremendously important to investigate the influence of aging on pyrotechnic compositions and assess the corresponding degradation processes.


Magnesium (Mg)-based pyrotechnic compositions are commonly employed as flares or tracers which provide high light output [9]. Tracers are usually employed to observe the ammunition trajectory during flight or to estimate the required correction to be applied for weapon systems. However, Mg-based pyrotechnic compositions (Mg-PCs) undergo degradation during storage, causing a malfunction of

the system or a change in performance [10]. Thus, the understanding of the aging processes of such compositions allows the control of their performance and ensures safe storage during its shelf life.

The development of effective approaches to evaluate the aging processes and the stability of energetic materials, e.g., propellants, explosives, and pyrotechnics is a hot topic, which has received much interest from the energetic community for several years, and will certainly continue to attract more attention in the future to find more efficient methodologies [8,11,12]. In the case of Mg-PCs, several authors have studied their aging behavior using thermal or non-thermal methods. Nevertheless, thermal analysis methods such as isothermal microcalorimetry, differential scan-

[a] S. Bekhouche, D. Trache, S. Chelouche, A. Abdelaziz, A. F. Tarchoun, W. Benchaa, S. Benameur, A. Mezroua  
Energetic Materials Laboratory, Teaching and Research unit of Energetic Processes, Ecole Militaire Polytechnique, BP 17 Bordj El-Bahri, 16046, Algiers, Algeria  
\*e-mail: djalaltrache@gmail.com

[b] A. F. Tarchoun  
Energetic Propulsion Laboratory, Teaching and Research unit of Energetic Processes, Ecole Militaire Polytechnique, BP 17 Bordj El-Bahri, 16046, Algiers, Algeria

 Supporting information for this article is available on the WWW under <https://doi.org/10.1002/prep.202100019>

ning calorimetry (DSC), modulated DSC, and thermogravimetry (TG) were the most employed ones for such purposes. Tuukkanen et al. studied the aging behavior of Mg-PCs supplemented with  $\text{Sr}(\text{NO}_3)_2$  as an oxidizer employing DSC and isothermal microcalorimetry [10,13,14]. The authors revealed that the presence of water vapor caused a direct reaction between Mg and  $\text{Sr}(\text{NO}_3)_2$ . The main reaction products were sodium nitrite magnesium hydroxide for which the amount increased with the progression of aging. In another work, De Klerk et al. assessed the aging behavior of Mg-PCs using TG for which the released gases during decomposition corresponded to  $\text{CO}_2$ , CO, and  $\text{N}_2\text{O}$ , with small amount of  $\text{NO}_2$ , NO, and HCN [15]. The authors found that the rise in the storage temperature could significantly increase the aging process. Recently, Babar et al. investigated the effect of the accelerated aging at  $70^\circ\text{C}$  and relative humidity of 70% on the behavior of Mg-based tracer composition [16]. The authors demonstrated that significant change in the thermal behavior was noticed for which the activation energy decreased with the progression of aging. These thermal analysis approaches are so important and can offer a good insight into the aging status of PCs. However, they may take much time to provide useful information. Thus, the use of simple, nondestructive, and effective methodologies based on spectroscopic tools such as FTIR and XRD could be interesting. The Batinić-Haberle research group studied the aging processes of Mg-PCs using IR and XRD to follow the eventual chemical changes that can occur [17,18]. The authors proved that artificial aging at higher temperatures and humidity reduces the stability of the pyrotechnic compositions. They attributed the interactions between metal and nitrate of the oxidizer to the chemical aging. However, their works do not allow an ease determination of the aging status of PCs, and thus updating data adopting effective and simple methodologies that provide better insight about the aging is more than necessary.

On the other hand, the complexity of the exploitation of the spectroscopic data for complex samples such as PCs because of the existence of different components that can generate overlapping and broad peaks and even undergo numerous complex phenomena pushed the scientific community to employ chemometric tools to overcome these drawbacks [19]. These latter have revealed their efficiency of discrimination and differentiations through the use of multivariate statistics, applied mathematics, and computer science to address issues in chemical engineering, biology, medicine, biochemistry, chemistry, and materials science [20,21]. Principal components analysis (PCA) is one of the powerful chemometric methods, which permits reducing multidimensional data into only few variables. This method can assist to discriminate and classify data to investigate specific behaviors such as material aging [22–24]. Recently, our research group combined spectroscopic methods coupled with PCA to detect eventual aging processes within energetic materials such as nitrocellulose and double base solid propellants [3,25,26]. The group has demonstrated

that such an approach is more effective to detect the aging status in an easy manner.

To the best of the author's knowledge, the combination of spectroscopic methods with chemometric tools such as PCA has never been applied to study the aging process of pyrotechnic compositions. Thus, this work focuses on the investigation of the effect of artificial thermal aging on the chemical structure and morphology of the Mg-PCs using Raman spectroscopy and SEM analysis. A deep study employing FTIR and XRD coupled with PCA has been undertaken to assess the possible discriminations of the obtained spectra and differentiate between unaged and thermally aged Mg-PCs.

## 2 Experimental Section

The tracer composition Mg-PCs (PTC) consisted of 61.5%  $\text{Sr}(\text{NO}_3)_2$  and 22.0% Mg supplied by Merck, 8.0% magnesium–aluminum alloy (50% Mg and 50% Al, mesh 300), and 8.5% phenolic resin purchased from Chengdu Huarui Industrial Co., Ltd.  $\text{Sr}(\text{NO}_3)_2$  was initially dried at  $80^\circ\text{C}$  and sieved through a  $125\text{ }\mu\text{m}$  mesh sieve before employment. The PTC was produced by blending the ingredients with phenolic resin solution for 30 min using a planetary mixer and passed through a  $375\text{ }\mu\text{m}$  sieve under humid conditions. The obtained mixture was then dried at  $60^\circ\text{C}$  for 8 h.

### 2.1 Accelerated Aging

Artificial aging experiments are carried out to get an insight about aging features in a relatively short cycle time, thus this approach permits saving a lot of time in investigations. Physical and/or chemical aging can be boosted by enhancing the storage temperature of the composition [26,27]. Despite no specific aging criteria for pyrotechnic compositions, in contrast to propellants, the aging tests of the PTC samples were performed at an isothermal temperature of  $65.5^\circ\text{C}$ , in an oven under ambient atmospheric conditions. The specimens were aged for a period of 4 months. The sampling was performed every 20 days during this period. A Fresh untreated sample served as a reference. All the samples were stored in vacuum desiccators to remove any residual or adsorbed water.

### 2.2 Analytical Techniques

The physical and chemical modifications during aging were assessed through FTIR and Raman spectroscopies, XRD, and scanning electron microscope (SEM).

FTIR spectra, recorded in transmission mode in the wavelength range of  $4000$  to  $400\text{ cm}^{-1}$ , were performed by KBr-technique on a Shimadzu spectrometer 8400S. A total of 32 scans was collected at room temperature to obtain a

high signal-to-noise ratio spectrum at a resolution of  $4\text{ cm}^{-1}$ . The spectra were subtracted against a background air spectrum. Identification was performed through a comparison of transmittance bands with those available in the literature.

The XRD diagrams were recorded using PANalytical X'Pert PRO powder diffractometer at a scan rate of  $0.04^\circ/\text{min}$  over the  $2\theta$  range of  $5$  to  $80^\circ$  using  $\text{Cu K}\alpha$  radiation and an X'celerator detector.

Raman spectra were acquired using Thermo-Fisher DXR 2 spectrometer.  $5\text{--}10\text{ mg}$  of samples were irradiated through a He–Ne laser of  $532\text{ nm}$  wavelength and  $30\text{ mW}$  power at room temperature.

The morphologies and compositions of the as-prepared PTC and its aged samples were characterized by SEM (Hitachi, model SUM800).

### 2.3 Sampling and Data Preprocessing

The FTIR patterns can be influenced by numerous factors such as the optical path length, the sample particle size, or its crystalline form, among others. Thus, an accurate sample preparation protocol and a meticulous analysis approach should be adopted. In addition, to decrease or eliminate any interference, mathematical pretreatments, which consist on smoothing using a derivative method (Savitzky-Golay method) and baseline correction, can be applied to the FTIR spectra. After this data transformation, centering (all columns should have mean zero) and scaling (the same variance) can also be required to improve the data presentation [19]. In the present work, data were scaled using Pareto method, the square root of the standard deviation as scaling factor  $\sqrt{S_i}$ , to reach equal effect of variable in a

Principal component analysis (PCA) [28–30]. A simplified workflow of data analysis and preprocessing is illustrated in Figure 1.

PCA, as the most utilized multivariate analysis tool [31], is a dimensionality-reduction process that is regularly employed to decrease the dimensionality of large data sets, by converting a large set of variables into a smaller one, which still encompasses most relevant information [32,33]. Accordingly, the new variables, named loadings, are linear combinations of the original ones and can be treated like new spectra [34].

### 2.4 Data Analysis

The collected spectra from  $4000\text{--}400\text{ cm}^{-1}$  wavenumbers on scale comprise 1868 data points. Data were consecutively organized as a matrix of dimensions  $7 \times 1868$  for which rows represent samples, whereas columns correspond to wavenumbers. Signal preprocessing, which involved the noise reduction and the background correction of the FTIR patterns, was accomplished in the wavelet domain [35–37].

### 2.5 Principal Component Analysis (PCA)

PCA is one of the multivariate data analysis techniques, which can be used to assess and visualize any interpretable and relevant structure in the data. In the present work, the analysis of data was performed through the statistical software PAST 3 program on the Windows platform. PCA is one of the most popular chemometrics methods. It is widely employed to decrease the data matrix dimension and com-

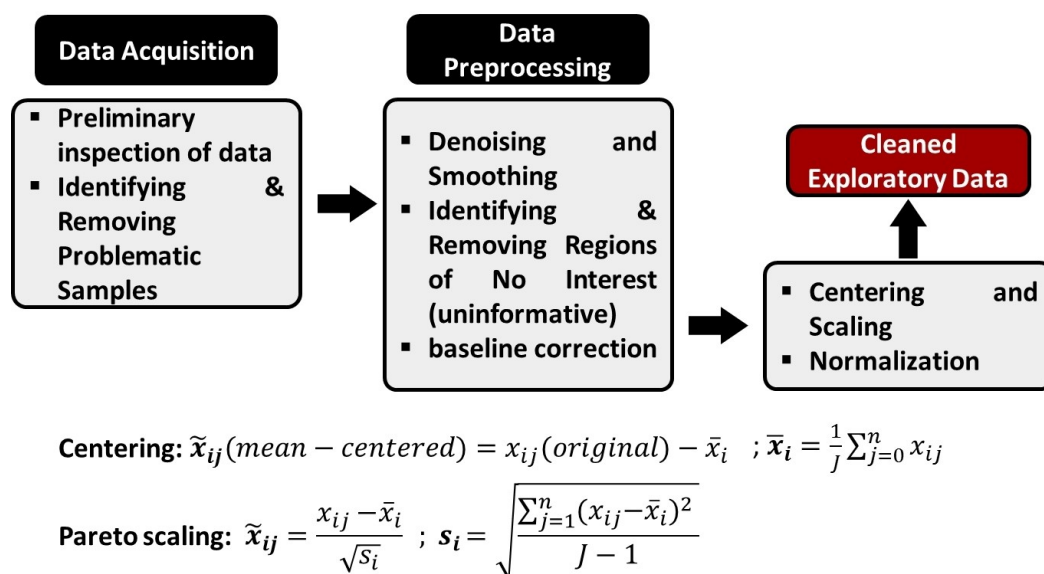


Figure 1. Simplified workflow of data analysis and preprocessing.

presses the details into a few new variables of data derived from spectroscopic analysis like FTIR and XRD [38–43]. It was utilized as an exploratory method, which allows the determination of the similarities and differentiation between the analysed samples, and permits identification of the influence of artificial aging on the physical and chemical features of pyrotechnic compositions. Typically, in PCA models, each cluster encompasses samples that have similar spectra and present similar characteristics, and therefore the farther the distance between clusters the more different they are [44].

The employment of PCA method allows converting the FTIR and XRD data matrices  $X$ , which encompass  $N$  lines (samples) and  $M$  columns (intensities) into two parameters. The first concerns the score matrix  $T$ , which is attributed to the sample coordinates in the new system of axes, whereas the second presents the loading matrix  $P$  assigned to the relation between the variables in addition to a residual matrix  $E$  [45]. Eq. 1 gives the mathematical presentation.

$$X = t_1 p_1^T + t_2 p_2^T + \dots + t_k p_k^T + E \quad (1)$$

The dimension for  $X$ ,  $T$ , and  $P$  are  $(N \times J)$ ,  $(N \times A)$ , and  $(A \times J)$ , respectively, with  $A$  is the number of principal components required to represent the convenient information in the data;  $N$  and  $J$  are the number of samples and variables, respectively, whereas  $E$  is the residual matrix, with same dimensions as  $X$ . This decomposition is particularly worthwhile to convert  $X$  to less informative plots (score plots and loadings plots) and for modeling the systematic structure in  $X$  as illustrated in Figure 2 [46, 47].

### 3 Results and Discussion

#### 3.1 Raman Analysis

For each PTC sample, five analyses were carried out and the averaged spectra were determined. Different preprocessing steps that involve smoothing, background correction, and normalization need to be made before spectrum analysis to eliminate/reduce noise and enhance the signal-to-noise ratio. Figure 3 displays the spectra obtained for the different PTC samples. The strong sharp Raman band in 1040–1060  $\text{cm}^{-1}$  region was assigned to the in-phase  $\text{NO}_3$  stretching vibrations of strontium nitrate [48]. Most bands are linked to the vibration modes of the anion  $\text{NO}_3^-$  of the  $\text{Sr}(\text{NO}_3)_2$  oxidizer, which is in good accordance with results from Barišin et al. [18, 49].

Figures 3 (I, II) and SM 1 (supporting materials) display a comparison of Raman spectra for fresh and aged compositions. Raman spectra of the aged samples unveil slight but critical intensity differences with respect to that of the unaged one. As can be seen in Figure 3 (II), a very weak band at  $\sim 1345 \text{ cm}^{-1}$  and a small shoulder at  $\sim 1570 \text{ cm}^{-1}$  are present. These peaks correspond to  $\text{NO}_2$  in-phase stretching vibration and the asymmetric stretch of the  $\text{NO}_3^-$  anion respectively, which can be attributed to the generation of strontium nitrite during aging that can subsequently affect the high temperature pyrotechnic reaction between magnesium and strontium nitrate [18, 50, 51]. Therefore, these changes may be caused by the partial decomposition of strontium nitrate and the oxidation of magnesium according to the following reactions [18, 49]:

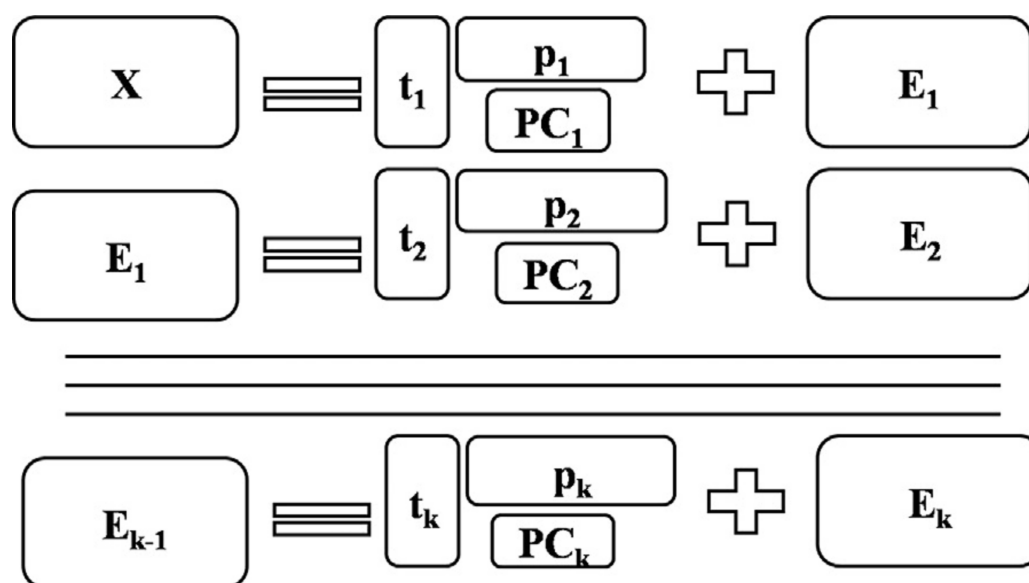


Figure 2. Schematic description of data matrix decomposition using PCA.

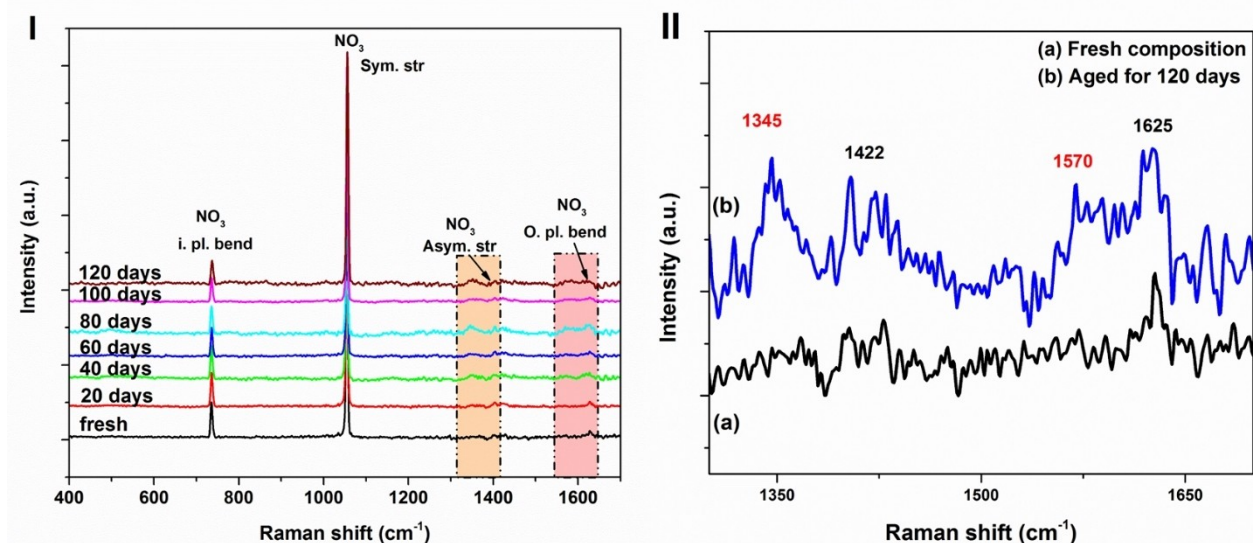
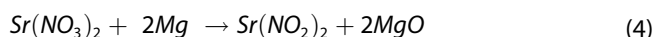
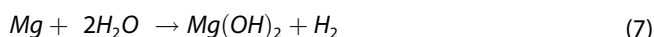


Figure 3. Raman spectra of fresh and aged PTC samples: (I) full range and (II) selected range.



The oxidation reactions of magnesium with the presence of humidity can occur as follows:



It is worthy to note that Raman spectroscopy appears less appropriate for detecting chemical modifications because the fluorescence background signal of the PTC is

more evident, as can be seen in Figure SM-1. This observation was also reported by Barišin [49]. Therefore, to confirm and explain the above-mentioned aging mechanism, it is more suitable to employ other analytical methods such as FTIR and XRD, as will be detailed.

### 3.2 FTIR and XRD Analyses

To investigate the chemical changes and elucidate the aging mechanism of PTC under accelerated conditions at high temperature, FTIR and XRD tools were used. Figure 4 depicts the FTIR spectra of all specimens for which the characteristic peaks of the different spectra are provided in Table 1. It is evident from Figure 4 that peak intensity changes are significant at some wavenumbers. Figure 5, however,

Table 1. FTIR characteristic peaks of PTC samples.

Wavenumber (cm <sup>-1</sup> )	Functional group vibration	References
3400	Stretching vibration of the linked O–H chemical group	[52,53]
2950	Stretching vibration of the linked O–H chemical group phenolic resin	[52]
2840–2770	$\nu_{42} + \nu_{32}$ asymmetric and symmetric NO <sub>3</sub> bending vibration	[54,55]
2445	$2 \nu_3$ NO <sub>3</sub> in-plane bending (2740–2760) cm <sup>-1</sup>	
2148	$\nu_1 + \nu_3$ asymmetric and symmetric NO <sub>3</sub> stretching vibrations	[56,57]
	$\nu_{12}$ NO <sub>3</sub>	[56,58]
	$\nu_{12}$ NO <sub>3</sub> 2105 cm <sup>-1</sup>	
	$\nu_{12}$ NO <sub>3</sub> 2138 cm <sup>-1</sup>	
	$2\nu_{32} + \nu_{31}$ NO <sub>3</sub> 2180 cm <sup>-1</sup>	
1790	$\nu_1 + \nu_4$ symmetric stretching and in-plane NO <sub>3</sub> bending vibrations	[56,57,59]
1444	$2 \nu_4$ NO <sub>3</sub> in-plane bending vibrations	[55]
1380	$\nu_3$ asymmetric stretching NO <sub>3</sub>	[48,55]
815	$\nu_2$ NO <sub>3</sub> out-of-plane bending vibrations	[56]
730	$\nu_4$ NO <sub>3</sub> in-plane bending vibrations	[55,57]



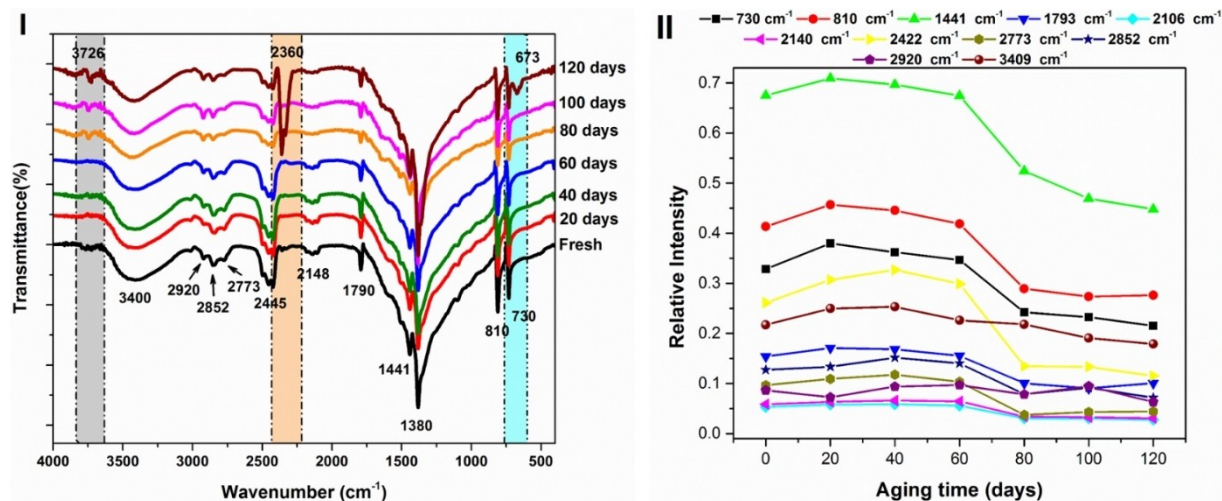


**Figure 4.** FTIR spectra of aged samples of PTC at 65 °C: (I) at different ageing times, (II) Variation of relative intensity of different FTIR bands with aging time.

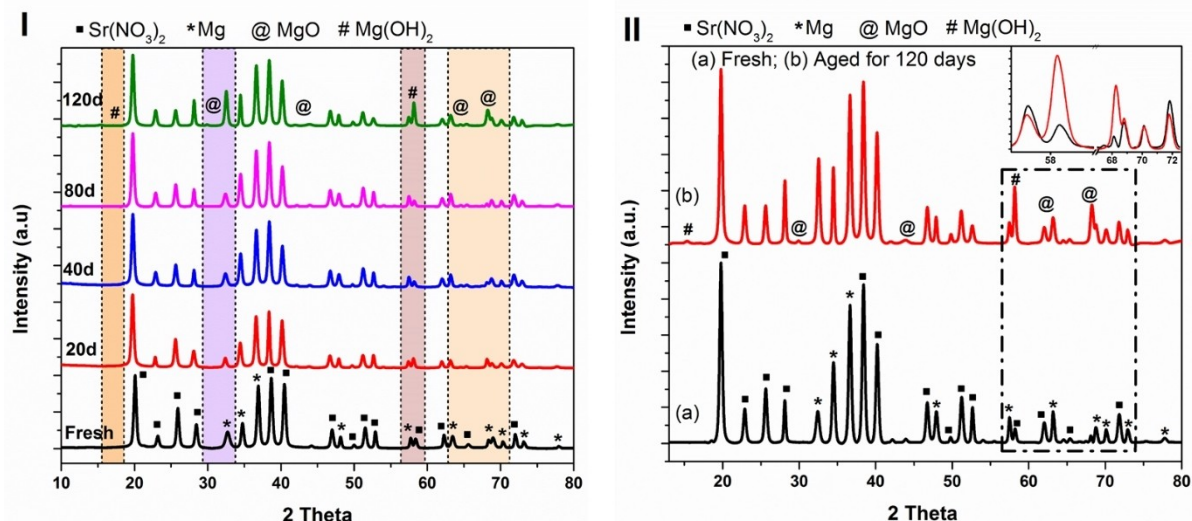


**Figure 5.** XRD patterns of PTC samples during accelerated aging: (I) at different aging times, (II) the fresh and aged samples.

displays the XRD pattern of the different specimens. These analyses allowed the characterization of the reaction products produced during the aging process.

As can be seen in Figure 4 (I), FTIR spectra of the different PTC samples displayed similar composition for which the transmittance bands are mainly attributed to the vibrations related to nitrates and linked O–H groups. Moreover, the small amount of magnesium, Mg–Al alloy, and the organic compound (phenolic resin) available within the mixture caused the absence or the overlapping of their respective transmittance bands [18]. The intense asymmetric stretching vibration detected at 1380 cm<sup>-1</sup> is assigned to nitrates, whereas a sharp medium-intense band that appeared at around 815 cm<sup>-1</sup> is attributed to the out-of-plane

bending vibration of NO<sub>3</sub>. The Raman active 730 cm<sup>-1</sup> and 1050 cm<sup>-1</sup> features (Figure 3) are much smaller in the IR spectra (Figure 4), these features correspond to the in-plane bending vibration and the symmetric stretching vibration of NO<sub>3</sub>, respectively. Moreover, a little-intense band at approximately 1790 cm<sup>-1</sup> can also be observed for these latter. Another weak band, which appeared at around 2440 cm<sup>-1</sup>, corresponds to the sum of the symmetric (1050 cm<sup>-1</sup>) and asymmetric (1380 cm<sup>-1</sup>) stretching vibrations of NO<sub>3</sub> [57]. The wide band that ranged from 2770 cm<sup>-1</sup> to 2920 cm<sup>-1</sup> could be attributed to combination tone or overtone asymmetric, symmetric stretching and bending vibrations of NO<sub>3</sub> [55], while that detected at 3400 cm<sup>-1</sup> is assigned to the stretching of OH group.

Besides that, a deep analysis of the FTIR spectra shown in Figures 4 (I) and SM-2 (supplementary materials) has been carried out. It can be seen that aging for 20, 40, and 60 days at 65 °C does not provoke any detectable chemical changes. Beyond 60 days, the changes become more visible, but significant changes appeared only when aging was performed at 65 °C for 120 days. Such modifications are mainly revealed by the appearance of the new bands at 3726 cm<sup>-1</sup>, 2360 cm<sup>-1</sup>, and 673 cm<sup>-1</sup>, respectively, which correspond to MgO stretching, Mg (OH)<sub>2</sub> stretching or NO<sub>2</sub> rocking bending vibrations. Accordingly, the above-mentioned discussion confirms the degradation of PTC during artificial aging, which is in good accordance with previous research activities [51,60,61].

Figure 4 (II) exhibits the evolution of the FITR relative peak intensities with aging time, which shows a small decrease in intensity for those of the aged samples compared to those of the unaged samples. In contrast, the samples aged for a period that exceeded 60 days display a rapid decrease in the relative intensity, what might be related to the high degradation rate of the aged PTC, revealing once again the influence of artificial aging. This decrease in the relative intensities of all the bands is more pronounced for the bands appearing at 730 cm<sup>-1</sup>, 810 cm<sup>-1</sup>, 1441 cm<sup>-1</sup>, and 2422 cm<sup>-1</sup>, that are the characteristic bands of NO<sub>3</sub> group, proving the partial decomposition of strontium nitrate to strontium nitrite during the aging process. These results corroborate with the literature data [13,18,50].

To identify the influence of aging time the relative intensities of the main FTIR bands associated with NO<sub>3</sub> groups of PTC samples, the relative intensities at 730 cm<sup>-1</sup>, 810 cm<sup>-1</sup>, 1441 cm<sup>-1</sup>, 1790 cm<sup>-1</sup> and 2422 cm<sup>-1</sup>, respectively, were plotted versus aging time, as depicted in Figure 4 (II). The experimental plots were fitted using MATLAB software based on the curve fitting approach for which numerous nonlinear models have been assessed.

The modeling parameters including the model coefficients and the regression quality for the different samples and various wavenumbers are summarized in Table 2. The results showed that the rational model (Eq. 8) was found to be the appropriate model that correlates well with the experimental data.

$$\text{Relative Intensity} = \frac{(p1 \times \text{Aging time}^2 + p2 \times \text{Aging time} + p3)}{(\text{Aging time}^2 + q1 \times \text{Aging time} + q2)} \quad (8)$$

Figure 5 shows the XRD pattern of the unaged (fresh) and aged PTC samples for which about twenty distinct peaks have appeared. Twelve peaks correspond to the characteristic peaks of strontium nitrate, whereas eight of them represent Mg. The diffraction pattern of MgO and Mg(OH)<sub>2</sub> peaks are obvious, indicating that a part of Mg available in the PTC sample has reacted with the water vapor to form magnesium hydroxide as a by-product of aging [18,50,60–

**Table 2.** The modeling parameters.

Wavenumber, cm <sup>-1</sup>	The modeling coefficients		Tolerance 95 %, confidence bounds	Regression quality Adjusted R-square	RMSE
730	p1	0.2562	(0.1539, 0.3585)	0.9840	0.01003
	p2	−0.1940	(−0.577, 0.189)		
	p3	0.2381	(−0.01963, 0.4958)		
	q1	−0.1945	(−1.554, 1.165)		
	q2	0.7049	(−0.09283, 1.503)		
810	p1	0.3505	(0.2459, 0.455)	0.9743	0.01379
	p2	−0.2620	(−0.7895, 0.2654)		
	p3	0.2014	(−0.03451, 0.4373)		
	q1	−0.3766	(−1.793, 1.04)		
	q2	0.4855	(−0.1037, 1.075)		
1441	p1	0.5588	(0.3762, 0.7414)	0.9770	0.01725
	p2	−0.4273	(−1.448, 0.5936)		
	p3	0.4806	(−0.1097, 1.071)		
	q1	−0.3867	(−2.131, 1.358)		
	q2	0.7266	(−0.2007, 1.654)		
1793	p1	0.1328	(0.09746, 0.1682)	0.9780	0.005262
	p2	−0.1076	(−0.2778, 0.06267)		
	p3	0.0616	(−0.005339, 0.1284)		
	q1	−0.4525	(−1.666, 0.7611)		
	q2	0.3978	(−0.04655, 0.8421)		
2422	p1	0.2162	(0.1124, 0.3201)	0.9727	0.01602
	p2	−0.2100	(−0.5253, 0.1052)		
	p3	0.1140	(−0.02033, 0.2483)		
	q1	−0.3623	(−1.635, 0.9104)		
	q2	0.3855	(−0.08786, 0.8589)		

62]. It is worthy to note that FTIR spectra also showed the existence of these Mg degradation by-products ( $\text{MgO}$  and  $\text{Mg}(\text{OH})_2$ ) in the aged PTC samples. These peaks were undetected in the X-ray diffractograms of the fresh PTC, demonstrating once more that accelerated aging influences the chemical composition of the pyrotechnic compositions.

As can be seen from Figure 5, the intensity of peaks at  $2\theta = 32.5^\circ$ ,  $58.2^\circ$ , and  $68.2^\circ$  increased with an increase in aging time, indicating a change in the structure of PTC samples. These peaks are prominently attributed to aging-related by-products overlapped by the peaks of PTC main components. Some authors attributed the degradation progress of pyrotechnics to the intimate interactions between metal and nitrate ions [17,18].

### 3.3 SEM Analysis

The SEM images (Figure 6) show the surface morphology of fresh and aged pyrotechnic compositions. The samples featured irregular shapes with sharp edges with some tendency to aggregate into large grains. At higher magnification ( $\times 3000$ ), the micrographs exhibit the formation of micro-cracks on the crystal surfaces of the aged compositions, elucidating the possible physicochemical changes during aging. The pristine sample displays a relatively smooth surface whereas the aged one shows an uneven surface and numerous cracks, which are located at the center of particles. The formed cracks could be attributed to the partial decomposition of the pyrotechnic composition promoted by the aging process. This outcome supports the above results of

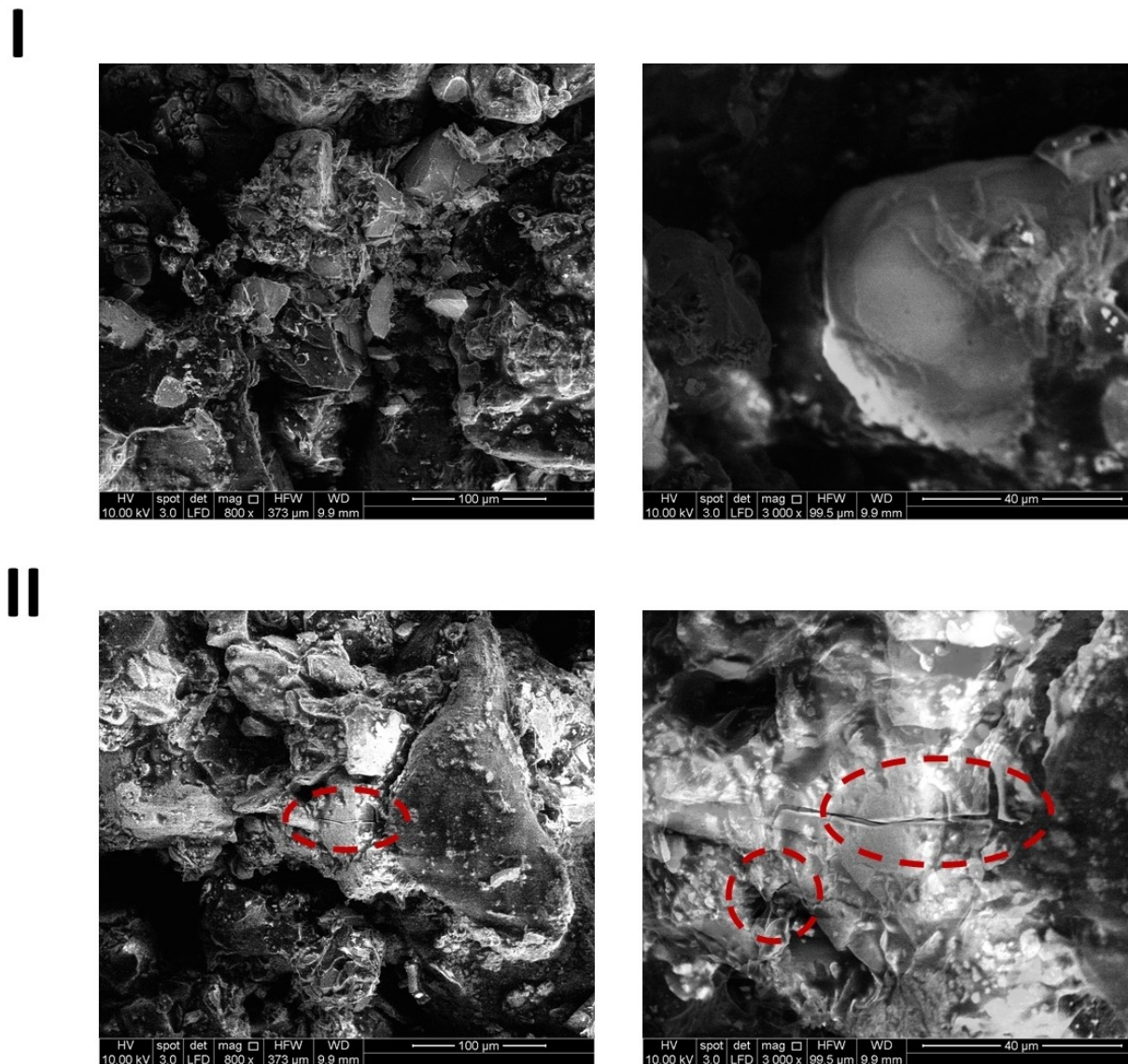


Figure 6. SEM micrographs of PTC samples: (I) fresh, (II) aged for 120 days.



FTIR and XRD analyses, which indicated that  $\text{Sr}(\text{NO}_3)_2$ ,  $\text{MgO}$ , and  $\text{Mg}(\text{OH})_2$  are the main products of degradation of PTC. Babar et al. have recently revealed a similar effect of thermal aging process on the morphology of pyrotechnic composition containing magnesium-sodium nitrate [16].

### 3.4 Chemometrics Analysis of the FTIR Results

The FTIR spectra of the different samples are broadly similar and overlay very well with each other (Figure SM-2). Their differences within the region  $400\text{--}4000\text{ cm}^{-1}$  of the spectra are not obvious. Accordingly, the PCA analysis was applied to ensure their differences and extract useful information. This methodology reveals the differences and similarities between sample spectra, and therefore detecting and classifying the sample patterns for better visualization and interpretation of the data [26,31,37].

Based on the total variance provided by the overall principal components (PCs) obtained from the whole data set (Table SM-1), the first two components, which present about 97.27% of the total variance, may correctly represent the data structure through their scores plot (PC1 and PC2). In Figure 7 (I), the PCA results (PC 1 versus PC 2 score plot) of the FTIR spectra, shows a clear differentiation between the fresh and aged PTC samples. As can be seen, the score values of samples increased by extending the accelerated aging time. Thus, the PTC had a tendency to move toward the positive PC1 values. It is obvious that the samples aged for a period not exceeding 60 days at  $65.5^\circ\text{C}$  are close to the fresh samples, revealing that the degradation of PTC is less pronounced. Nonetheless, the fresh PTC sample (0 d) is different from the aged ones (20 d, 40 d, and 60 d), which is

certainly caused by certain physicochemical changes, as confirmed by the above Raman, FTIR, XRD, and SEM analyses. Moreover, the extension of the aging time to a period that surpasses 60 days at  $65.5^\circ\text{C}$  intensify the degradation of the PTC, which is demonstrated by a fast increase in PC1, revealing the high decomposition rate. These findings corroborate well with the FTIR spectra and XRD diffractograms.

On the other hand, it is worthy to mention that, in multivariate data analysis, samples with close features and similar properties show clusters, whereas those with different characteristics will appear different from the groups [19]. Therefore, a low similarity signifies a large distance between sample spectra in the scatter plot of the scores (PC1 versus PC2). According to the scatter plot, three groups (I, II, and III) of spectra, that are separated along PC1, can be identified. These groups demonstrate that FTIR is effective in detecting modification caused by the thermal aging process. Each group displays similar features, which change with aging as follows: group I (aging time  $\leq 60$  d), group II ( $60\text{ d} < \text{aging time} \leq 100$  d), and group III (aging time  $\geq 120$  d). Such modification can be assigned to the interactions between strontium nitrate and magnesium, as proved by the FTIR and XRD data.

Figure 7 (II) shows the loading plots vs wavenumbers, corresponding to contribution of original wavenumbers to the different principal components (PCs) [26]. The corresponding loading plot presents the link between the scores of the PCs and the intensities of the FTIR spectra, allowing the determination of the bands that exhibit an intense variation during aging [19]. The PC1 and PC2 loading plots reflect the effect of artificial aging on the different samples for which the main peaks are at  $734\text{ cm}^{-1}$ ,  $815\text{ cm}^{-1}$ ,  $1385\text{ cm}^{-1}$ ,  $1441\text{ cm}^{-1}$  and  $1791\text{ cm}^{-1}$ , corresponding to  $\text{O--NO}_2$  blending, symmetric and

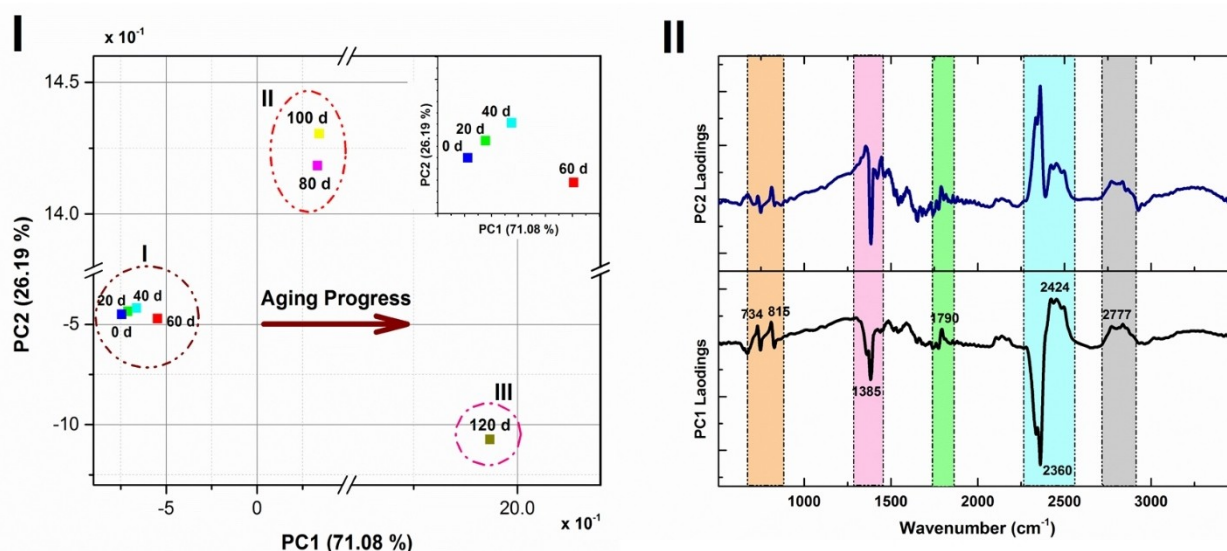


**Figure 7.** (I) Scatter plot of the scores from PC 1 and PC 2 determined using FTIR data of fresh and aged samples, (II) loadings plot, PC 1 and PC2 versus wavenumbers.

asymmetric stretching vibrations, respectively, are the most influenced bands by the aging process.

### 3.5 Chemometrics Analysis of the XRD Results

The results of the variances obtained using the XRD data revealed that the first three PC factors present the most of variances between the fresh and artificially aged PTC samples (more than 97%). Figures 8 (I) and SM-4 exhibit the scores plot of the first three components. Based on PC1 scores that decrease with the increase of aging process, an obvious difference between the fresh and aged samples can be seen. The samples, which present close PCA scores are much more similar than the other samples, revealing the modification of the structure of PTC during aging. Moreover, the fresh samples and those aged 20 d and 40 d with almost the same XRD data belong to the same clusters, revealing that less change of the structure has occurred. However, the extension of the aging causes an intense change in the PTC structure, and hence the scores of the aged samples for 60 d, 80 d, 100 d and 120 d are more distant from the fresh ones, confirming once more the accuracy of the proposed degradation mechanism obtained with Raman, FTIR, and XRD data. Moreover, the PC1, PC2 and PC3 loading plots (Figure 8 (II)) reveal the influence of artificial aging on the different samples and show that the structure of the PTC samples has changed after aging. Subsequently, the employment of these spectroscopic methods coupled with PCA is a prominent approach for the investigation of the degradation of pyrotechnic compositions. All the findings reported above prove the effectiveness of FTIR and XRD combined to chemometrics to study various characteristics of energetic materials.

## 4 Conclusions

As far as we know, this is the first work dealing with the investigation of the thermal aging behavior of the pyrotechnic composition based on strontium nitrate and magnesium using FTIR and XRD combined with PCA. The developed approach allowed the classification of composite tracer composition aged for different periods at 65.5 °C. The chemical groups of the main PTC ingredients have been monitored with aging and a mathematical model has been effectively employed to support the discussion of the FTIR spectra.

The experimental results confirmed that the non-destructive spectroscopy techniques FTIR, Raman spectroscopy, and XRD offered suitable information about the chemical changes of the pyrotechnic composition during artificial aging. The obtained FTIR spectra displayed a decrease in the intensities of the mean bands with the extension of aging time. Moreover, this attenuation in the relative intensities of all the bands is more obvious after 60 days of aging.

Furthermore, the XRD spectra of the CTPs exhibited the effect of the accelerated aging on their structure, which indicated that the intensity of peaks at  $2\theta = 32.5^\circ$ ,  $58.2^\circ$ , and  $68.2^\circ$  was found to increase with the aging time. These diffractograms were prominently attributed to aging products overlapped by the peaks of other components, for which the reaction between metal and nitrate ions is considered crucial in the degradation progress.

Lastly, multivariate data analysis of spectroscopic methods is demonstrated to be an interesting approach to characterize the pyrotechnic composition for which the aging process can be easily detected. Overall, the present activity points out the importance of the combination of spectroscopic methods with chemometric tools to assist the available methods to evaluate the pyrotechnic composition aging.

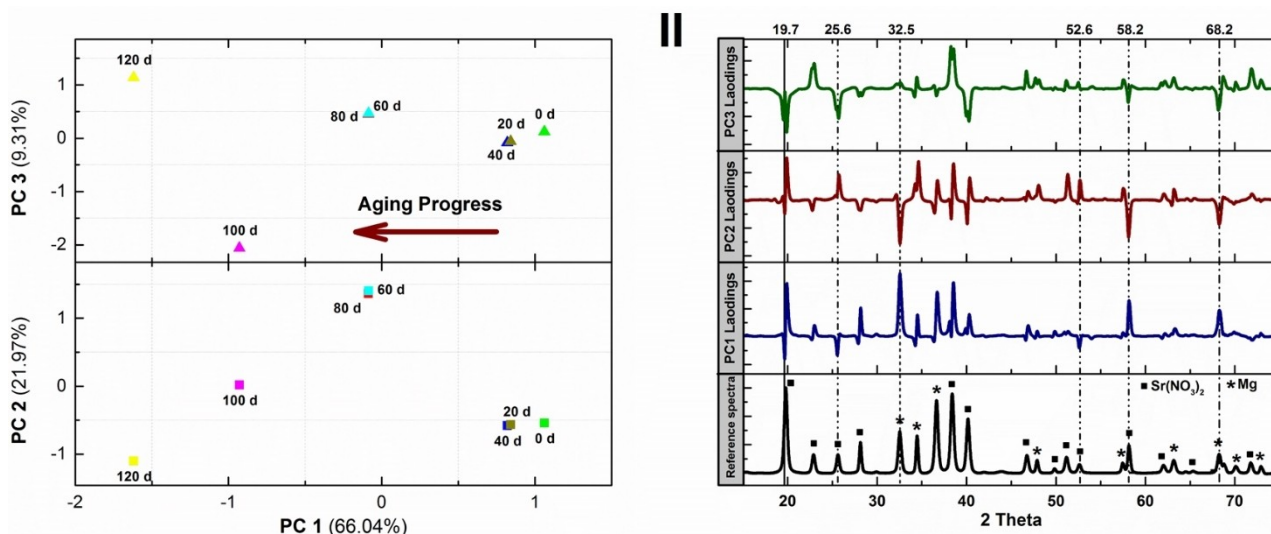


Figure 8. (I) PCA scatter plot of XRD spectra, (II) loadings plot, PC 1, PC2, and PC3 versus 2θ values.

## Data Availability Statement

The data that support the findings of this study are available from the corresponding author upon reasonable request.

## References

- [1] S. Danali, R. Palaiah, K. Raha, Developments in pyrotechnics, *Def. Sci. J.* **2010**, *60*, 152–158.
- [2] J. S. Brusnahan, A. P. Shaw, J. D. Moretti, W. S. Eck, Periodates as potential replacements for perchlorates in pyrotechnic compositions, *Propellants Explos. Pyrotech.* **2017**, *42*, 62–70.
- [3] S. Chelouche, D. Trache, A. F. Tarchoun, K. Khimeche, A. Mezroua, Stability Assessment for Double Base Rocket Propellant During Long Natural/Artificial Aging Using Various Methods and Kinetic Modeling, in *Materials Research and Applications*, Springer, **2021**, pp. 93–122.
- [4] D. Trache, A. Mazroua, K. Khimeche, Determination of chemical and mechanical properties of propellants during ageing, *Proceedings of 42nd international annual conference of ICT*, Karlsruhe **2011**, 83.
- [5] S. Chelouche, D. Trache, A. F. Tarchoun, K. Khimeche, Effect of organic eutectic on nitrocellulose stability during artificial aging, *J. Energ. Mater.* **2019**, *37*, 387–406.
- [6] L. Wang, X. Shi, W. Wang, The influences of combinative effect of temperature and humidity on the thermal stability of pyrotechnic mixtures containing strontium nitrate as oxidizer, *J. Therm. Anal. Calorim.* **2014**, *117*, 985–992.
- [7] A. Q. Malik, Investigation of the thermal decomposition of magnesium–sodium nitrate pyrotechnic composition (SR-524) and the effect of accelerated aging, *J. Saudi Chem. Soc.* **2017**, *21*, 262–269.
- [8] G. Manton, Accelerated Ageing of Pyrotechnics: Evaluation of Pyrotechnic Degradation, in *Ageing Studies and Lifetime Extension of Materials*, Springer, **2001**, pp. 619–626.
- [9] H. Pouretedal, S. L. Mousavi, Study of the ratio of fuel to oxidant on the kinetic of ignition reaction of  $Mg/Ba(NO_3)_2$  and  $Mg/Sr(NO_3)_2$  pyrotechnics by non-isothermal TG/DSC technique, *J. Therm. Anal. Calorim.* **2018**, *132*, 1307–1315.
- [10] I. Tuukkanen, E. L. Charsley, S. Goodall, P. G. Laye, J. J. Rooney, T. T. Griffiths, H. Lemmetyinen, An investigation of strontium nitrite and its role in the ageing of the magnesium–strontium nitrate pyrotechnic system using isothermal microcalorimetry and thermal analysis techniques, *Thermochim. Acta.* **2006**, *443*, 116–121.
- [11] D. Trache, A. F. Tarchoun, Analytical methods for stability assessment of nitrate esters-based propellants, *Crit. Rev. Anal. Chem.* **2019**, *49*, 415–438.
- [12] A. Benhammada, D. Trache, Thermal decomposition of energetic materials using TG-FTIR and TG-MS: a state-of-the-art review, *Appl. Spectrosc. Rev.* **2020**, *55*, 724–777.
- [13] I. Tuukkanen, S. Brown, E. L. Charsley, S. Goodall, P. G. Laye, J. J. Rooney, T. T. Griffiths, H. Lemmetyinen, A study of the influence of the fuel to oxidant ratio on the ageing of magnesium–strontium nitrate pyrotechnic compositions using isothermal microcalorimetry and thermal analysis techniques, *Thermochim. Acta.* **2005**, *426*, 115–121.
- [14] I. Tuukkanen, S. Brown, E. L. Charsley, S. Goodall, J. Rooney, T. T. Griffiths, H. Lemmetyinen, Studies on the ageing of a magnesium–strontium nitrate pyrotechnic composition using isothermal microcalorimetry and thermal analysis techniques, *Thermochim. Acta.* **2004**, *417*, 223–229.
- [15] W. De Klerk, W. Colpa, P. Van Ekeren, Ageing studies of magnesium–sodium nitrate pyrotechnic compositions, *J. Therm. Anal. Calorim.* **2006**, *85*, 203–207.
- [16] Z.-u.-d. Babar, A. Q. Malik, Investigation of the thermal decomposition of magnesium–sodium nitrate pyrotechnic composition (SR-524) and the effect of accelerated aging, *J. Saudi Chem. Soc.* **2017**, *21*, 262–269.
- [17] D. Barišin, I. Batinić-Haberle, Aging of Pyrotechnic Compositions. The investigation of chemical changes by IR spectroscopy and x-ray diffraction, *Propellants Explos. Pyrotech.* **1989**, *14*, 162–169.
- [18] I. Batinić-Haberle, D. Barišin, I. Spasojevic, Z. Vranic, The stability characterization of the pyrotechnic system. The degradation of the nitrate oxidant in the presence of the magnesium under the accelerated aging conditions, *Propellants Explos. Pyrotech.* **1992**, *17*, 10–13.
- [19] K. Varmuza, P. Filzmoser, *Introduction to multivariate statistical analysis in chemometrics*, CRC press, **2016**.
- [20] R. G. Brereton, J. Jansen, J. Lopes, F. Marini, A. Pomerantsev, O. Rodionova, J. M. Roger, B. Walczak, R. Tauler, Chemometrics in analytical chemistry—part II: modeling, validation, and applications, *Anal. Bioanal. Chem.* **2018**, *410*, 6691–6704.
- [21] M. Khanmohammadi, *Current Applications of Chemometrics*, Nova Science Publishers, Incorporated, **2014**.
- [22] D. Song, J. Gao, X. Li, L. Lu, Evaluation of aging behavior of polypropylene in natural environment by principal component analysis, *Polym. Test.* **2014**, *33*, 131–137.
- [23] S. Chelouche, D. Trache, I. Maamache, A. F. Tarchoun, K. Khimeche, A. Mezroua, A new experimental way for the monitoring of the real/equivalent in-service-time of double base rocket propellant by coupling VST and PCA, *Def. Tech.* **2020**.
- [24] J. Lever, M. Krzywinski, N. Altman, Points of significance: Principal component analysis, *Nature method* **2017**, *14*, 641–642.
- [25] D. Trache, A. F. Tarchoun, Differentiation of stabilized nitrocellulose during artificial aging: Spectroscopy methods coupled with principal component analysis, *J. Chemom.* **2019**, *33*, e3163.
- [26] S. Chelouche, D. Trache, Z. I. Benayachi, A. F. Tarchoun, K. Khimeche, A. Mezroua, A New Procedure for Stability Control of Homogeneous Solid Propellants by Combination of Vacuum Stability Test, FTIR and PCA, *Propellants Explos. Pyrotech.* **2020**.
- [27] J. L. de la Fuente, An analysis of the thermal aging behaviour in high-performance energetic composites through the glass transition temperature, *Polym. Degrad. Stab.* **2009**, *94*, 664–669.
- [28] R. A. van den Berg, H. C. Hoefsloot, J. A. Westerhuis, A. K. Smilde, M. J. van der Werf, Centering, scaling, and transformations: improving the biological information content of metabolomics data, *BMC Genomics* **2006**, *7*, 142.
- [29] R. Bro, A. K. Smilde, Principal component analysis, *Anal. Methods* **2014**, *6*, 2812–2831.
- [30] K. Wang, Y. Yuan, S. Han, H. Yang, Application of attenuated total reflectance Fourier transform infrared (ATR-FTIR) and principal component analysis (PCA) for quick identifying of the bitumen produced by different manufacturers, *Road Mater. Pavement Des.* **2018**, *19*, 1940–1949.
- [31] J. Zhang, Analysis and characterization of consumer products by FTIR, Raman, chemometrics, and two dimensional ATR-FTIR correlation spectroscopy, The State University of New Jersey (Rutgers), **2009**.
- [32] H. Martens, M. Martens, Multivariate analysis of quality. An introduction, *Meas. Sci. Technol.* **2001**, *12*, 1746.

- [33] H. Martens, T. Ni, *Multivariate calibration*, John Wiley & Sons, 1992.
- [34] Y. Roggo, P. Chalus, L. Maurer, C. Lema-Martinez, A. Edmond, N. Jent, A review of near infrared spectroscopy and chemometrics in pharmaceutical technologies, *J. Pharm. Biomed. Anal.* **2007**, 44, 683–700.
- [35] S. Zhou, Q. Yin, L. Lu, Z. Wang, G. Deng, Application of near infrared spectroscopy in fast assay of liquid components in single-base propellant intermediates, *Infrared Phys. Technol.* **2017**, 80, 11–20.
- [36] M. López-López, V. Merk, C. García-Ruiz, J. Kneipp, Surface-enhanced Raman spectroscopy for the analysis of smokeless gunpowders and macroscopic gunshot residues, *Anal. Bioanal. Chem.* **2016**, 408, 4965–4973.
- [37] D. Trache, A. F. Tarchoun, Differentiation of stabilized nitro-cellulose during artificial aging: Spectroscopy methods coupled with principal component analysis, *J. Chemom.* **2019**, 33, e3163.
- [38] R. Kumar, V. Kumar, V. Sharma, Fourier transform infrared spectroscopy and chemometrics for the characterization and discrimination of writing/photocopier paper types: Application in forensic document examinations, *Spectrochim. Acta Part A* **2017**, 170, 19–28.
- [39] Y. Otsuka, A. Ito, S. Matsumura, M. Takeuchi, S. Pal, H. Tanaka, Quantification of pharmaceutical compounds based on powder X-ray diffraction with chemometrics, *Chem. Pharm. Bull.* **2016**, 64, 1129–1135.
- [40] J. Dadson, S. Pandam, N. Asiedu, Modeling the characteristics and quantification of adulterants in gasoline using FTIR spectroscopy and chemometric calibrations, *Cogent Chem.* **2018**, 1482637.
- [41] L. Bertacchini, C. Durante, A. Marchetti, S. Sighinolfi, M. Silvestri, M. Cocchi, Use of X-ray diffraction technique and chemometrics to aid soil sampling strategies in traceability studies, *Talanta* **2012**, 98, 178–184.
- [42] Y. Zhou, B. Li, P. Zhang, Fourier transform infrared (FT-IR) imaging coupled with principal component analysis (PCA) for the study of photooxidation of polypropylene, *Appl. Spectrosc.* **2012**, 66, 566–573.
- [43] L. De Oliveira, A. Antunes, M. Bueno, Direct chromium speciation using X-ray spectrometry and chemometrics, *X-Ray Spectrom.* **2010**, 39, 279–284.
- [44] S. M. Obeidat, I. Al-Momani, A. Haddad, M. Bani Yasein, Combination of ICP-OES, XRF, and XRD techniques for analysis of several dental ceramics and their identification using chemometrics, *J. Spectrosc.* **2011**, 26, 141–149.
- [45] M. Ferreira, A. M. Antunes, M. S. Melgo, P. L. Volpe, Chemometrics I: multivariate calibration, a tutorial, *Quim. Nova* **1999**, 22, 724–731.
- [46] A. C. Pereira, M. S. Reis, P. M. Saraiva, J. C. Marques, Analysis and assessment of Madeira wine ageing over an extended time period through GC–MS and chemometric analysis, *Anal. Chim. Acta* **2010**, 660, 8–21.
- [47] N. Kumar, A. Bansal, G. Sarma, R. K. Rawal, Chemometrics tools used in analytical chemistry: An overview, *Talanta* **2014**, 123, 186–199.
- [48] F. Zapata, C. García-Ruiz, The discrimination of 72 nitrate, chlorate and perchlorate salts using IR and Raman spectroscopy, *Spectrochim. Acta Part A* **2018**, 189, 535–542.
- [49] D. Barišin, I. Batinić-Haberle, Aging of Pyrotechnic Compositions. The investigation of chemical changes by IR spectroscopy and X-ray diffraction, *Propellants Explos. Pyrotech.* **1989**, 14, 162–169.
- [50] S. Brown, E. L. Charsley, S. Goodall, P. G. Laye, J. J. Rooney, T. T. Griffiths, Studies on the ageing of magnesium–potassium nitrate pyrotechnic composition using isothermal heat flow calorimetry and thermal analysis techniques, *Thermochim. Acta* **2003**, 401, 53–61.
- [51] I. Tuukkanen, S. Brown, E. L. Charsley, S. Goodall, P. G. Laye, J. J. Rooney, T. T. Griffiths, H. Lemmetyinen, A study of the influence of the fuel to oxidant ratio on the ageing of magnesium–strontium nitrate pyrotechnic compositions using isothermal microcalorimetry and thermal analysis techniques, *Thermochim. Acta* **2005**, 426, 115–121.
- [52] B. C. Smith, *Fundamentals of Fourier transform infrared spectroscopy*, CRC press, 2011.
- [53] P. Larkin, *Infrared and Raman spectroscopy: principles and spectral interpretation*, Elsevier, 2017.
- [54] K. Nakamoto, *Infrared and Raman Spectra of Inorganic and Coordination Compounds, Theory and Applications in Inorganic Chemistry*, Wiley-Interscience, 1997.
- [55] F. El-Kabbany, S. Taha, M. Tosson, IR Spectral Analysis of the Mixed Crystal System of  $\text{AgNO}_3$  and  $\text{Sr}(\text{NO}_3)_2$ , *Ann. Phys.* **1989**, 501, 569–577.
- [56] C. Schutte, The crystal structures and infra-red spectra of barium and strontium nitrates, *Z. Kristallogr.* **1968**, 126, 397–402.
- [57] N. He, Y. Ni, J. Teng, H. Li, L. Yao, P. Zhao, Identification of inorganic oxidizing salts in homemade explosives using Fourier transform infrared spectroscopy, *Spectrochim. Acta Part A* **2019**, 221, 117164.
- [58] C. J. H. Schutte, The influence of coupling on the  $\text{NO}_3^-$ -vibrations in  $\text{Ba}(\text{NO}_3)_2$  and  $\text{Sr}(\text{NO}_3)_2$  with special reference to the overtone and combination bands, *Zeitschrift für Phys. Chemie* **1963**, 39, 241–248.
- [59] R. A. Nyquist, R. O. Kagel, *Handbook of infrared and raman spectra of inorganic compounds and organic salts: infrared spectra of inorganic compounds, Vol. 4*, Academic press, 2012.
- [60] D. Barišin, I. Batinić-Haberle, P. Jovanić, Aging of pyrotechnic composition. The reliability of X-ray diffraction data for estimation of the quality of signal mix, *Propellants Explos. Pyrotech.* **1989**, 14, 255–259.
- [61] W. de Klerk, E. Krabbendam-LaHaye, B. Berger, H. Brechbuhl, C. Popescu, Thermal studies to determine the accelerated ageing of flares, *J. Therm. Anal. Calorim.* **2005**, 80, 529–536.
- [62] Z. u. d. Babar, A. Q. Malik, Accelerated ageing of SR-562 pyrotechnic composition and investigation of its thermo kinetic parameters, *Fire Mater.* **2017**, 41, 131–141.

Manuscript received: January 20, 2021  
Revised manuscript received: March 23, 2021  
Version of record online: April 15, 2021